Electronic Supplementary Information

Ultrafast excited state relaxation dynamics in heteroleptic Ir(III) complex, *fac*-Ir(ppy)$_2$(ppz), revealed by femtosecond x-ray transient absorption spectroscopy

Jungkweon Choi,[a,b] Mina Ahn,[c] Jae Hyuk Lee,[d] Doo-Sik Ahn,[a,b] Hosung Ki,[a,b] Inhwan Oh,[b] Chi Woo Ahn,[b] Eun Hyuk Choi,[b] Yunbeom Lee,[b] Seonggon Lee,[b] Jungmin Kim,[b] Dae Won Cho,[e] Kyung-Ryang Wee,[c,*] Hyotcherl Ihee[a,b,*]

a. Center for Nanomaterials and Chemical Reactions, Institute for Basic Science, Daejeon 34141, Republic of Korea
b. Department of Chemistry and KI for the BioCentury, Korea Advanced Institute of Science and Technology (KAIST), Daejeon 34141, Republic of Korea
c. Department of Chemistry, Daegu University, Gyeongsan 38453, Republic of Korea
d. Pohang Accelerator Laboratory, Pohang, 37673, Republic of Korea
e. Department of Advanced Materials Chemistry, Korea University, Sejong Campus, Sejong 30019, Korea

* Corresponding author: Kyung-Ryang Wee and Hyotcherl Ihee
E-mail: krwee@daegu.ac.kr, hyotcherl.ihee@kaist.ac.kr

Experimental Section

1. Synthesis. All of the synthesis procedures were performed under a dry argon condition. Reagents and solvents were obtained from Sigma-Aldrich, Duksan Company, and OCI company Ltd., and used without further purification. Deuterated solvent for NMR experiments was obtained from Merck or Cambridge Isotope Lab. Inc. Silica gel column chromatography was performed on silica gel 60 G (230–400 mesh ASTM, Merck Co.). The synthesized compounds were characterized by ^{1}H-NMR or ^{13}C-NMR, mass spectroscopy, and elemental analysis. The ^{1}H and proton decoupled ^{13}C spectra were recorded on a Bruker500 spectrometer operating at 500 and 125 MHz, respectively, and all proton and carbon chemical shifts were measured relative to internal residual chloroform (99.9 % $CDCl_3$) or dimethyl sulfoxide (99.8 % DMSO-d_6) from the lock solvent. The elemental analyses (C, H, N) were performed using Thermo Fisher Scientific Flash 2000 series analyzer. As shown in Scheme S1, the final Ir(III) complexes, containing cyclometalating ligands ((C^N) 2-phenylpyridine (ppy) and (C^N)′ 1-phenylpyrazole (ppz)), were synthesized through the two-step reactions starting from synthesis of di-μ-chloride−iridium dimer precursor. The synthesis of the neutral tris-cyclometalated Ir(III) complex allowed forming two geometric configurations, facial (*fac*) and meridional (*mer*) isomers. The facial form was thermodynamically controlled, and the meridional form was kinetically controlled. By regulating the reaction temperature, the facial isomer was favorably produced as the main product. The meridional product was converted to their facial product under the high reaction temperature condition.

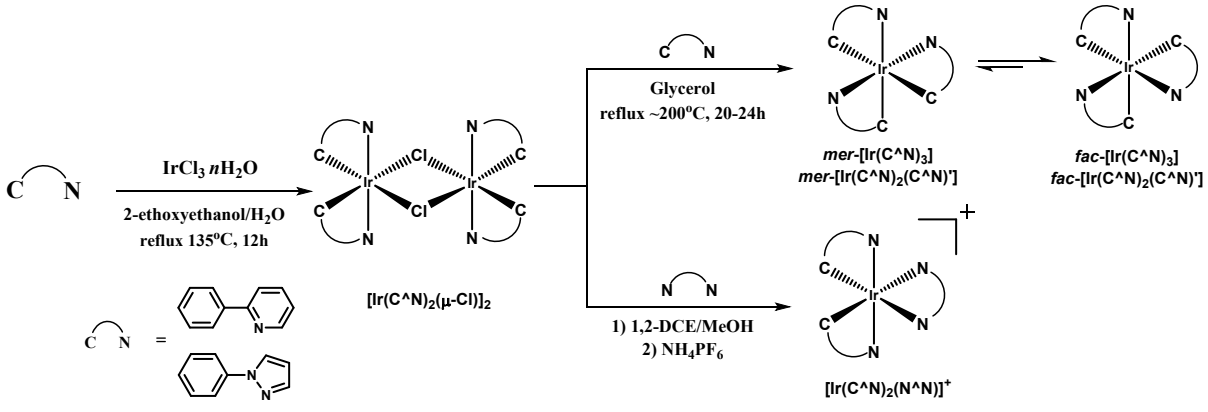

Scheme S1. Synthesis route of Ir(III) dimer and Tris-cyclometalated Ir(III) complexes.

2. Synthesis of $[Ir(C^N)_2(\mu\text{-}Cl)]_2$ Complexes. The dichloro-bridged iridium dimer complexes $[Ir(C^N)_2(\mu\text{-}Cl)]_2$ were prepared based on the previously published method.[1, 2]

$[Ir(ppy)_2(\mu\text{-}Cl)]_2$ Tetrakis(2-phenylpyridine-*N,C*$^{2'}$) (μ-dichloro)diiridium: Yield: 85 %, yellow brown powder. ^{1}H-NMR (500 MHz, $CDCl_3$, ppm) δ 9.26 (d, 4H), 7.89 (d, 4H), 7.76 (t, 4H), 7.51 (d, 4H), 6.81-6.75 (m, 8H), 6.58 (t, 4H), 5.95 (d, 4H).

$[Ir(ppz)_2(\mu\text{-}Cl)]_2$ Tetrakis(1-phenylpyrazole-*N,C*$^{2'}$) (μ-dichloro)diiridium: Yield: 79 %, light gray powder. ^{1}H-NMR (500 MHz, $CDCl_3$, ppm) δ 8.06 (d, 4H), 7.78 (d, 4H), 7.03 (d, 4H), 6.70 (t, 4H), 6.58 (t, 4H), 6.46 (t, 4H), 5.94 (d, 4H).

3. Synthesis of *fac*-$[Ir(ppy)_3]$ and *fac*-$[Ir(ppz)_3]$ of the type $[Ir(C^N)_3]$, and *fac*-$[Ir(ppy)_2(ppz)]$ of the type *fac*-$[Ir(C^N)_2(C^N)']$ complexes. Homoleptic and Heteroleptic Tris-cyclometalated Iridium(III) Complexes were synthesized via a slight modification of the method reported by Tamayo.[3] A mixture of $[Ir(C^N)_2(\mu\text{-}Cl)]_2$, cyclometalating ligand, and K_2CO_3 were heated to ~200 °C under argon in glycerol for 20-24 h. After cooling to room temperature, 20 mL of deionized H_2O was added, and the resulting precipitate was filtered off, washed with methanol, and followed by ether and hexane. The crude product was purified through a silica plug using CH_2Cl_2 eluent. The final product was further purified by recrystallization from a mixture of EtOAc and hexane followed by a mixture of CH_2Cl_2 and hexane.

***fac*-$[Ir(ppy)_3]$ *fac*-tris(2-(phenyl)pyridinato-*N,C*$^{2'}$) iridium(III) complex:** Yield: 80 %, yellow powder. ^{1}H-NMR (500 MHz, DMSO-d_6, ppm) δ 8.14 (d, 3H), 7.80 (t, 3H), 7.76 (d, 3H), 7.49 (d, 3H), 7.14 (t, 3H), 6.81 (t, 3H), 6.71-6.65 (m, 6H). ^{13}C{^{1}H} (125 MHz, DMSO-d_6, ppm) δ 166.1, 161.2, 147.3, 144.3, 137.4, 136.8, 129.5, 124.6, 123.3, 120.0, 119.5. Anal. Calcd for $C_{33}H_{24}IrN_3$: C, 60.53; H, 3.69; N, 6.42. Found: C, 60.51; H, 3.60; N, 6.42.

***fac*-$[Ir(ppz)_3]$ *fac*-tris(1-phenylpyrazolato-*N,C*$^{2'}$) iridium(III) complex:** Yield: 78 %, white powder. ^{1}H-NMR (500 MHz, DMSO-d_6, ppm) δ 8.65 (d, 3H), 7.50 (d, 3H), 7.00 (d, 3H), 6.87-6.84 (m, 3H), 6.67-6.65 (m, 6H), 6.56 (t, 3H). ^{13}C{^{1}H} (125 MHz, DMSO-d_6, ppm) δ 144.2, 139.4, 136.9, 136.6, 126.7, 125.2, 120.3, 111.4, 107.3. Anal. Calcd for $C_{27}H_{21}IrN_6$: C, 52.16; H, 3.40; N, 13.52. Found: C, 52.10; H, 3.38; N, 13.52.

***fac*-[Ir(ppy)$_2$(ppz)] *fac*-bis(2-phenylpyridinato-*N*,*C*$^{2'}$)(1-phenylpyrazolate-*N*,*C*$^{2'}$) iridium(III) complex[4]:** Yield: 60 %, yellow powder. ^{1}H-NMR (500 MHz, DMSO-d_6, ppm) δ 8.69-8.66 (m, 1H), 8.15-8.10 (m, 2H), 7.83-7.78 (m, 2H), 7.76-7.74 (m, 2H), 7.59-7.55 (m, 1H), 7.52-7.48 (m, 2H), 7.19-7.08 (m, 2H), 6.96-6.91 (m, 1H), 6.85-6.79 (m, 3H), 6.76-6.71 (m, 2H), 6.70-6.64 (m, 3H), 6.62-6.60 (m, 1H), 6.58-6.57 (m, 1H). ^{13}C{^{1}H} (125 MHz, DMSO-d_6, ppm) δ 166.6, 166.4, 165.8, 159.2, 147.9, 146.8, 144.6, 144.5, 144.4, 142.8, 137.7, 137.5, 137.3, 137.1, 136.8, 136.4, 129.5, 127.4, 125.8, 125.7, 124.6, 124.5, 123.3, 122.8, 120.6, 120.1, 119.5, 119.2, 111.9, 108.3, 107.8. Anal. Calcd for $C_{31}H_{23}IrN_4$: C, 57.84; H, 3.60; N, 8.70. Found: C, 57.80; H, 3.58; N, 8.73.

4. Ultrafast optical transient absorption spectroscopy. Transient absorption (TA) spectra were measured with femtosecond laser pulses using a visible pump–broadband probe scheme. The output pulses at a wavelength of 800 nm from a Ti:sapphire amplified laser (Coherent Legend Elite) were split into the pump and probe beams. On the pump arm, the laser pulses of 800 nm were converted into the pump pulses of the wavelength of 400 nm using a second harmonic generation (SHG) BBO crystal. The pulse energy of the pump pulses was 500 nJ, providing a fluence of ~57 μJ/mm^2. On the probe arm, the laser pulses at 800 nm were sent into a c-cut sapphire window of 3 mm thickness and converted into a white light continuum spanning from visible to near-infrared wavelengths by self-phase modulation. The visible portion (460 – 725 nm) of the white light continuum was used as broadband probe pulses without further compensation of the dispersion. The probe pulses were time-delayed with respect to the pump pulses using a motorized translation stage (Newport, M-ILS150HA). By recording the "pump-on" and "pump-off" probe spectra, the differential transmission (ΔT/T) spectrum was obtained as a function of the delay time. The spectra of transient signal and the reference were detected by a spectrometer (Andor, SR303i) equipped with a Si CCD (Andor, DU420A). The temporal resolutions of our femtosecond TA systems is about 150 fs. In all the measurements, the polarization of the pump pulses was set to be at the magic angle (54.7°) relative to the probe polarization in order to prevent polarization-dependent signals. For the TA measurement, *fac*-Ir(ppy)$_2$(ppz) was dissolved in acetonitrile. *fac*-Ir(ppy)$_2$(ppz) solution in acetonitrile was prepared with an optical density of ~0.4 at 400 nm in acetonitrile in a 1 mm glass cuvette.

5. Femtosecond x-ray transient absorption spectroscopy. The femtosecond x-ray transient absorption measurements were performed at the XSS beamline of PAL-XFEL. The sample solution of 1.5 mM *fac*-Ir(ppy)$_2$(ppz) in acetonitrile (Aldrich, anhydrous, 99.8%) was circulated through a quartz capillary nozzle of 100 μm thickness to provide a fresh sample for each pair of laser and x-ray pulse. The open jet capillary system with a thickness of 100 μm provides a stable flow of liquid with a speed fast enough to deliver a fresh sample solution at every pump-probe measurement at a repetition rate of 30 Hz. Optical laser pulses with the center wavelength of 400 nm were generated by second harmonic generation (SHG) of the 800-nm femtosecond laser pulses, which were provided by a 15 Hz amplified Ti:sapphire laser system, and was used as the pump to initiate the photochemical reaction. The temporal resolutions of the fs-XTA systems is about 150 fs. The 400 nm optical laser pulses were focused on a 0.5 (width) × 0.5 (height) mm^2 spot at the sample position, providing a fluence of ~1.5 mJ/mm^2. The sample concentration in acetonitrile was adjusted to be ~0.8 mM. The laser and x-ray pulses will be aligned in a collinear geometry with a crossing angle of 10 degrees to maximize the spatial overlap between the two pulses and minimize the velocity mismatch. X-ray pulses with photon energies near the Ir L_{III}-edge (11.2 keV) will be used to obtain a transient x-ray absorption signal after the excitation of the sample solution. To assemble a transient x-ray absorption spectrum, x-ray absorption for Ir L_{III}-edge was measured as a function of the photon energy of probe x-ray with the avalanche photodiode by the total fluorescence yield method. The x-ray spot size was 50 × 50 μm^2 at the sample position.

6. Calibration of XTA spectra of *fac*-Ir(ppy)$_2$(ppz): To compensate systematic errors in XTA experiments, XTA spectra of *fac*-Ir(ppy)$_2$(ppz) are calibrated using that of reference sample, *fac*-Ir(ppy)$_2$(bpy). As shown in Fig S14, XTA spectrum of *fac*-Ir(ppy)$_2$(bpy) measured in this study exhibits a weak intensity compared to the previously reported spectrum of *fac*-Ir(ppy)$_2$(bpy)[5]. The intensity discrepancy between two spectra at each x-ray energy was calibrated with a scaling factor defined as follows.

$$\text{Scaling factor (x-ray energy)} = \text{Intensity}_{\text{known curve}} / \text{Intensity}_{\text{measured curve}}$$

Using the obtained scaling factor, XTA spectra of *fac*-Ir(ppy)$_2$(ppz) measured at Δt = 0.5 and 3 ps were calibrated as depicted in Fig. S15. Reconstructed XTA spectra of *fac*-Ir(ppy)$_2$(ppz) were used throughout the analysis.

7. Density functional theory (DFT) and Time-dependent DFT (TDDFT) calculations: The optimized ground-state structures of *fac*-Ir(ppy)$_3$, *fac*-Ir(ppz)$_3$ and *fac*-Ir(ppy)$_2$(ppz) were obtained from DFT calculations using the CAM-B3LYP functional with def2-SVP basis sets, and they were additionally confirmed with a larger def2-TZVP basis sets. To simulate UV absorption curves of three species, 100 vertical transition energies were calculated using TDDFT method with the same functional and basis sets, while the optimized structure of *fac*-Ir(ppy)$_2$(ppz) in S_1 state was obtained by calculating the analytical TDDFT energy gradient of S_1 state. Similarly, the optimized geometries of T_1 and T_2, the ground and the first excited triplet state, were calculated by the same DFT and TDDFT methods, respectively. Solvent effects of acetonitrile in all calculations were treated by using the conductive polarizable continuum model (CPCM). The minimum and transition states were confirmed by vibrational normal mode analysis. All calculations were performed using Gaussian 16 (version B.01) software.[6]

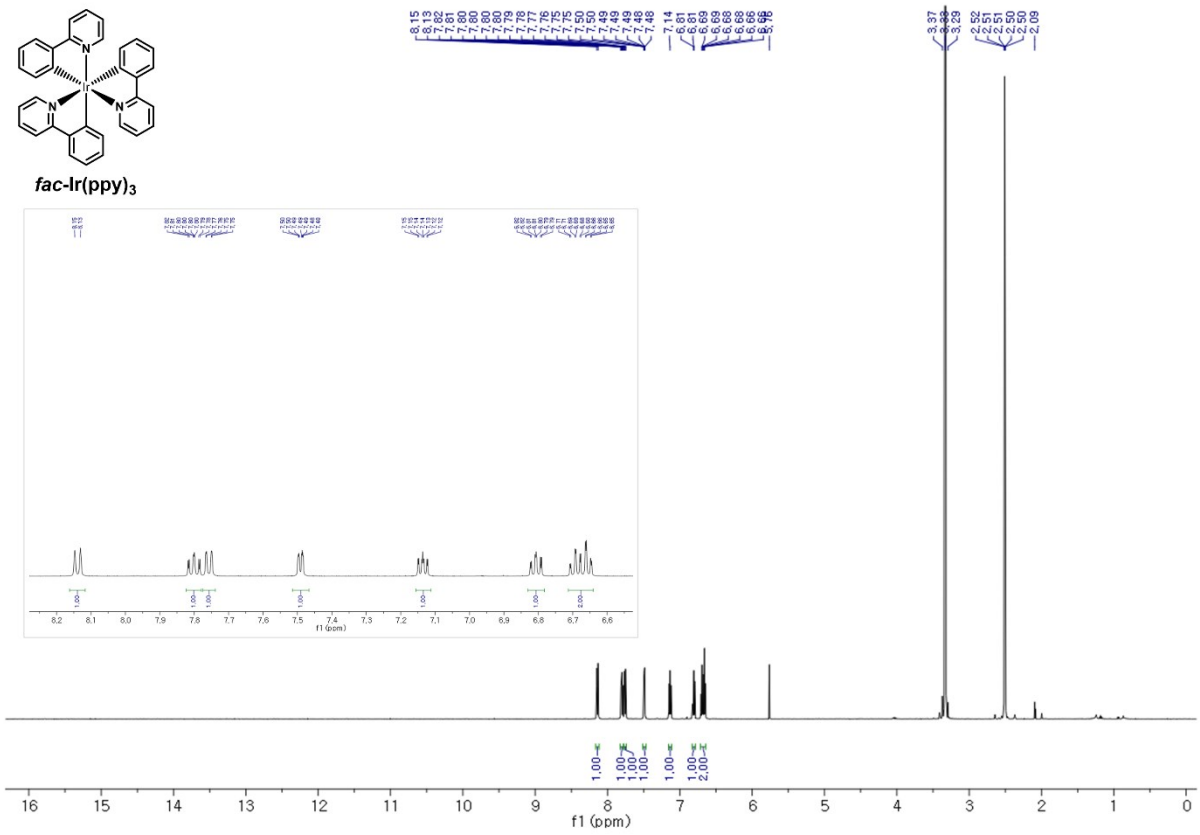

Fig. S1. ^{1}H-NMR spectrum of *fac*-[Ir(ppy)$_3$] in DMSO-d_6 (500MHz, 293K).

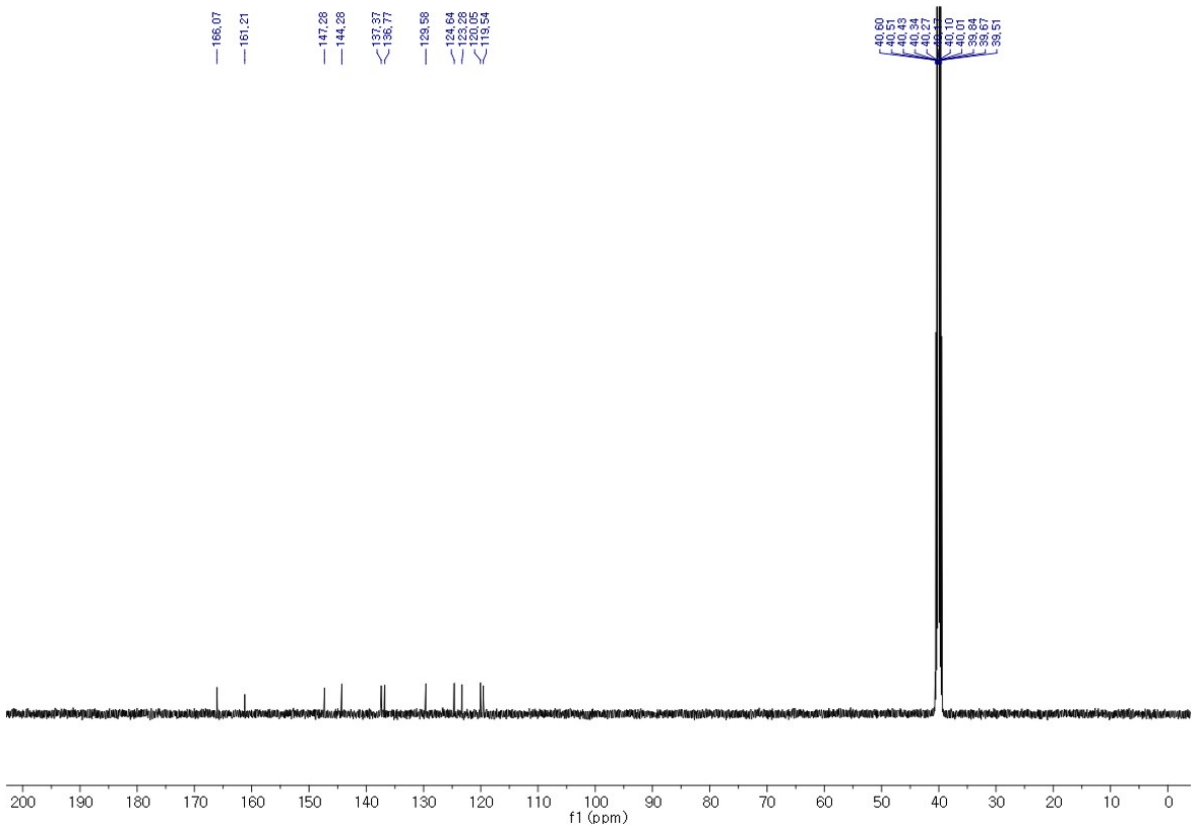

Fig. S2. ^{13}C-NMR spectrum of *fac*-[Ir(ppy)$_3$] in DMSO-d_6 (125MHz, 293K).

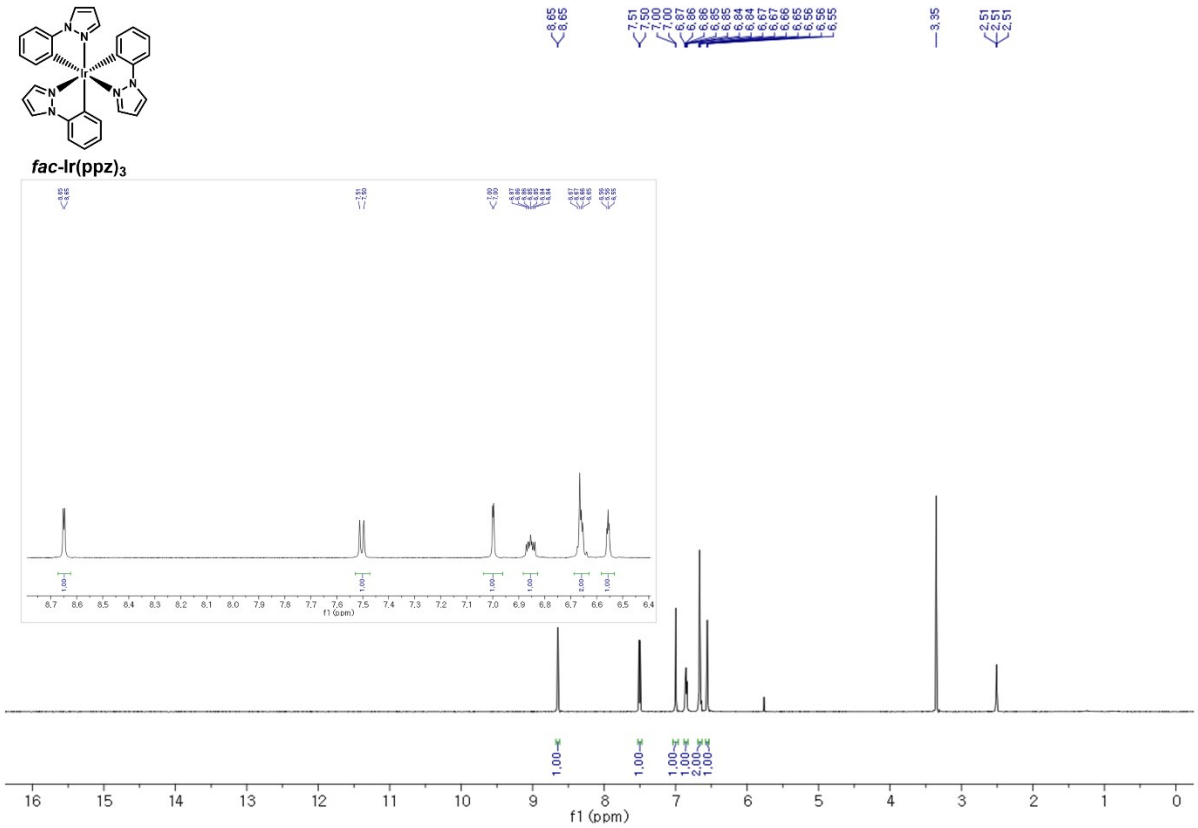

Fig. S3. ^{1}H-NMR spectrum of *fac*-[Ir(ppz)$_3$] in DMSO-d_6 (500MHz, 293K).

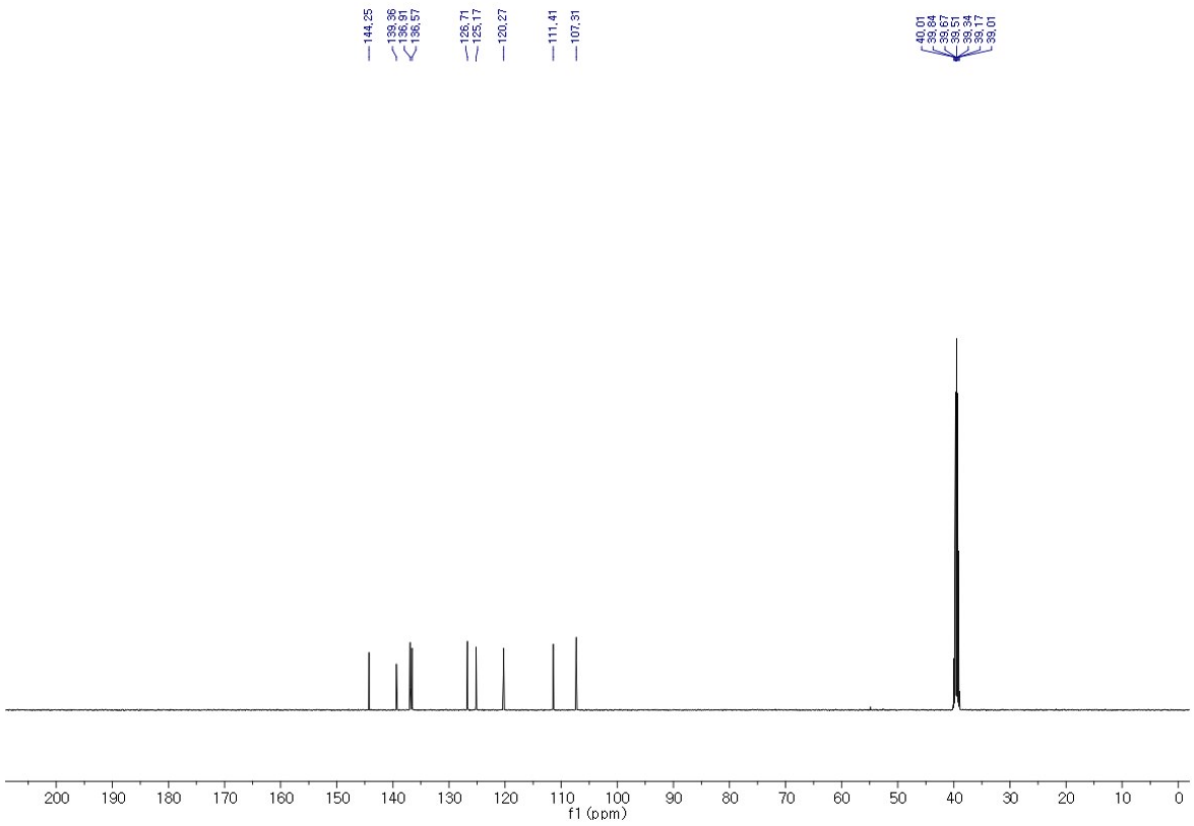

Fig. S4. ^{13}C-NMR spectrum of *fac*-[Ir(ppz)$_3$] in DMSO-d_6 (125 MHz, 293 K).

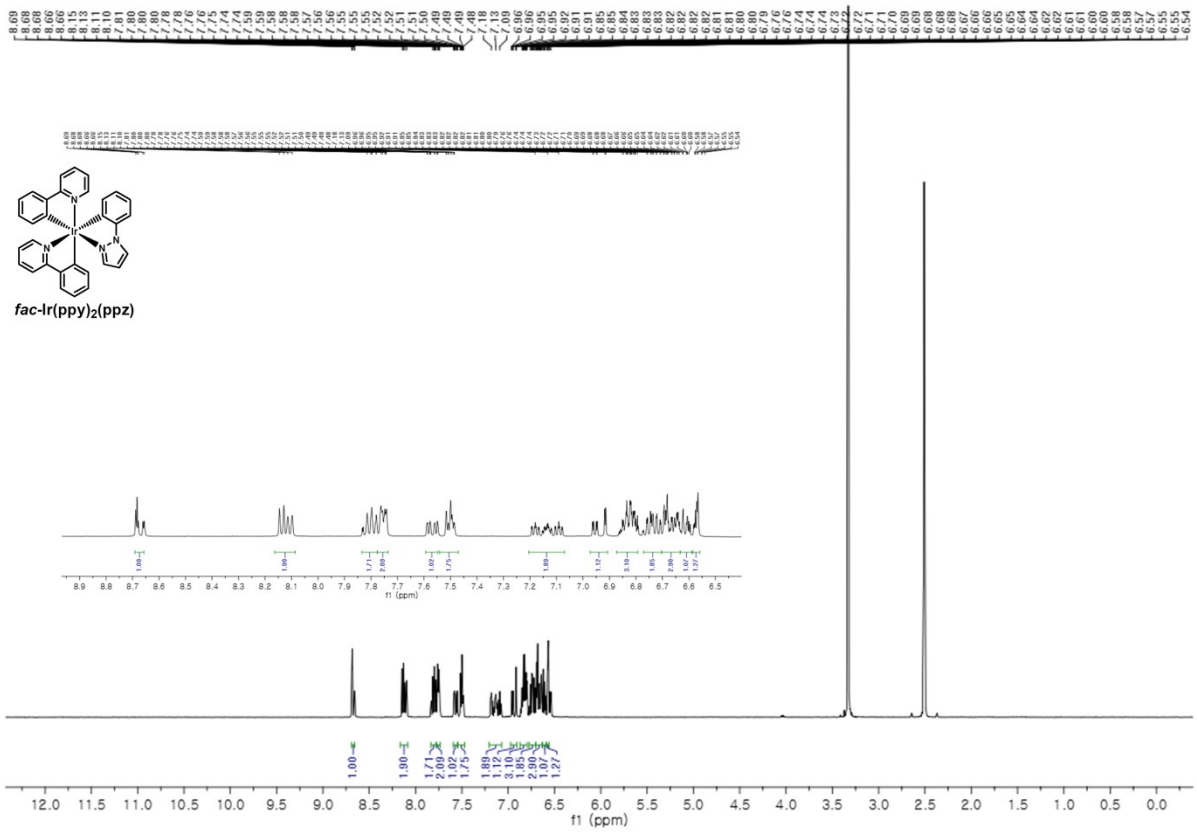

Fig. S5. ^{1}H-NMR spectrum of *fac*-[Ir(ppy)$_2$(ppz)] in DMSO-d_6 (500MHz, 293K).

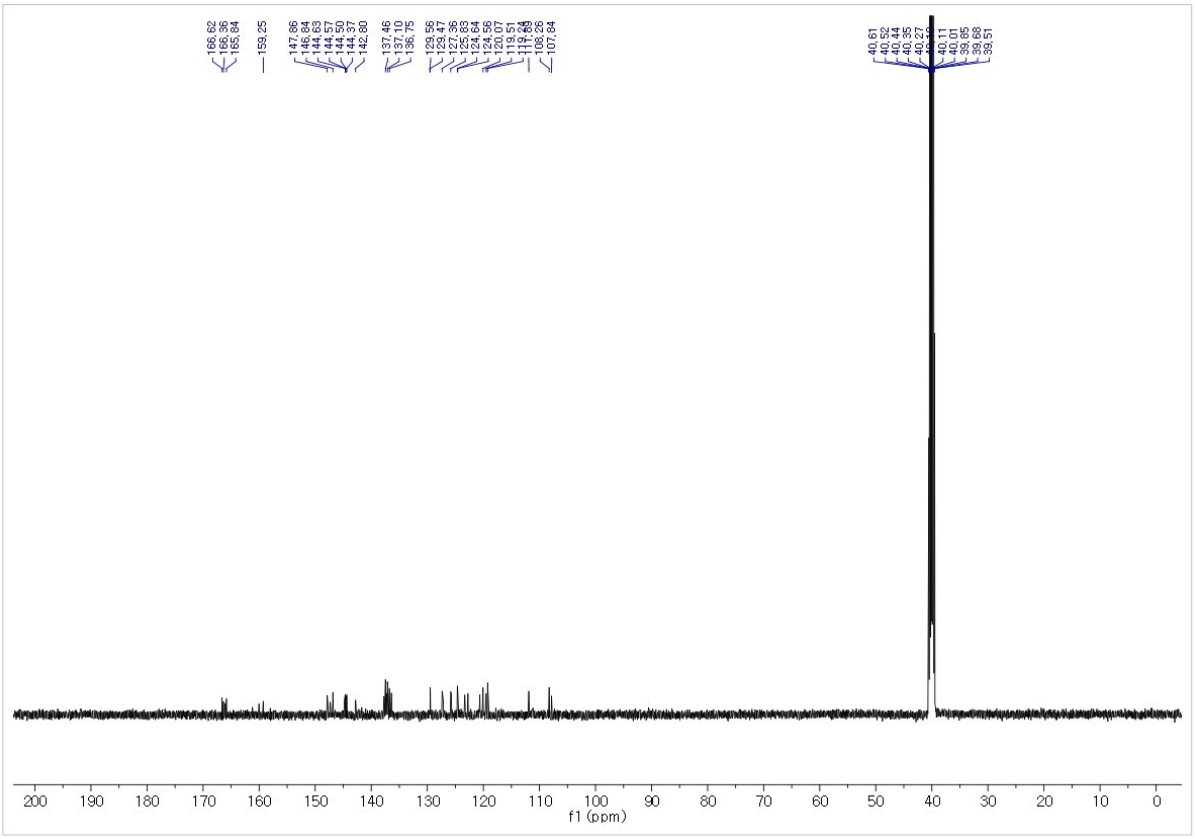

Fig. S6. ^{13}C-NMR spectrum of *fac*-[Ir(ppy)$_2$(ppz)] in DMSO-d_6 (125MHz, 293K).

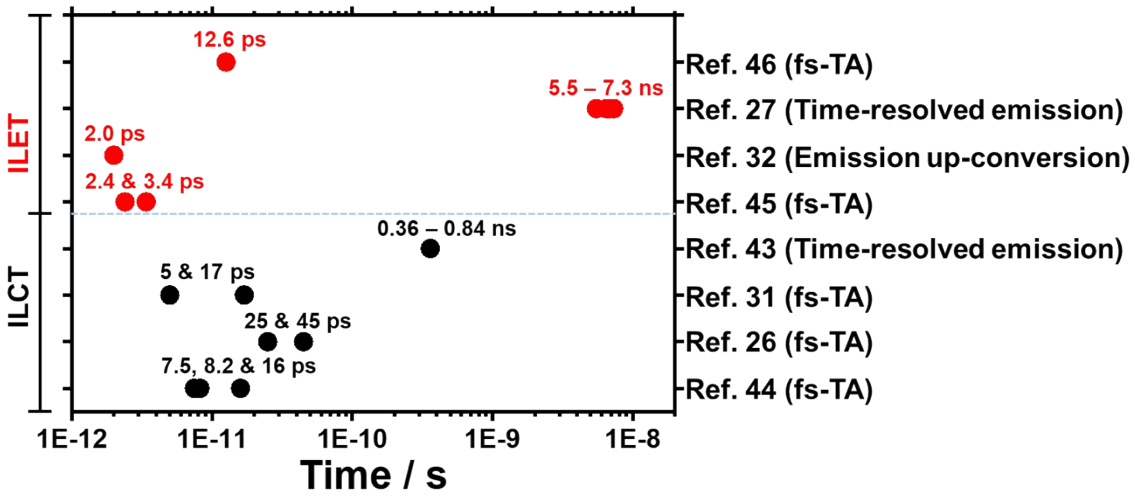

Fig. S7. Comparison of the excited state relaxation dynamics of Ir(III) complexes using various time-resolved techniques. The numbers on the right side indicate the reference numbers.

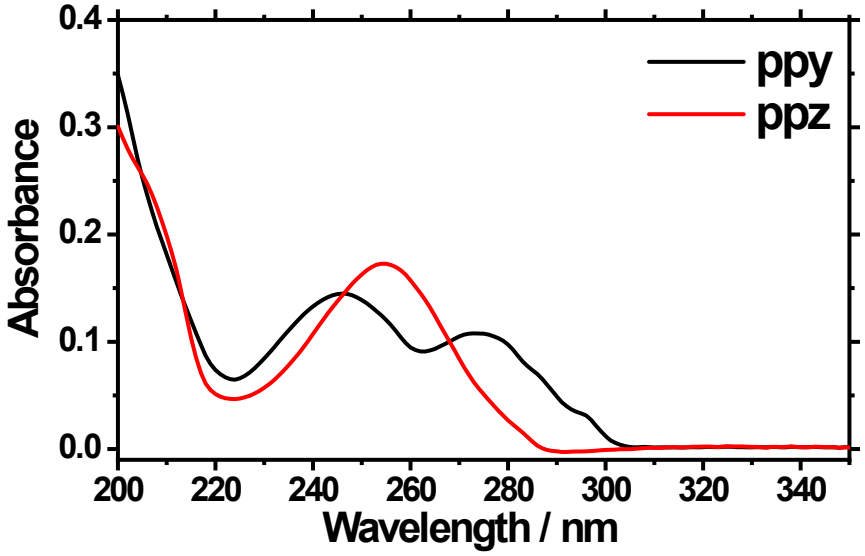

Fig. S8. UV-visible absorption spectra of ppy and ppz ligands in acetonitrile.

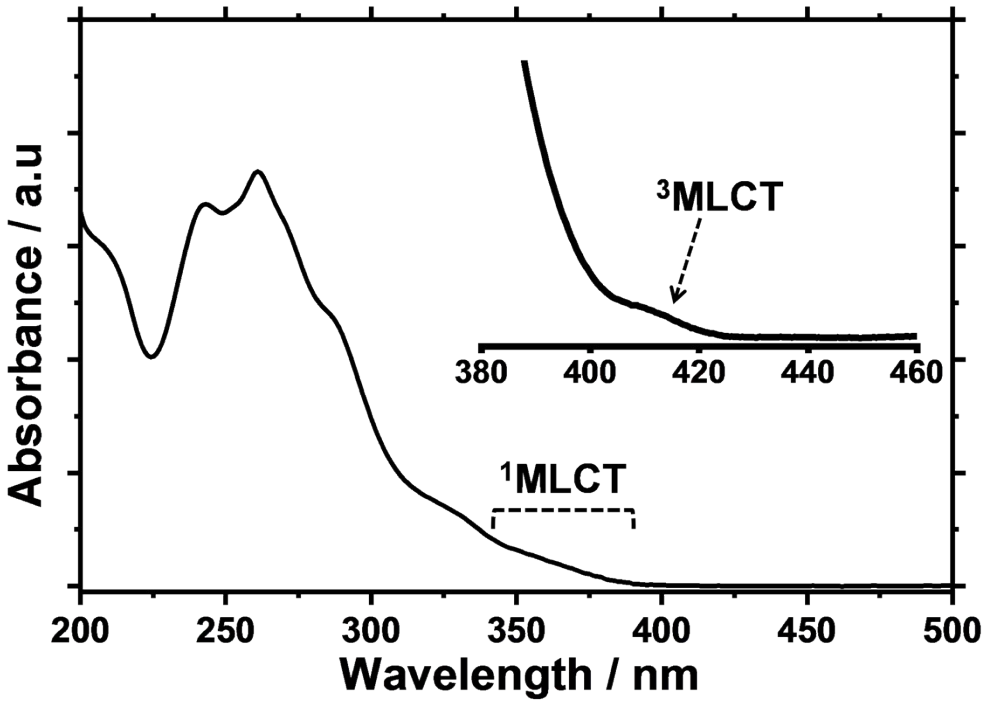

Fig. S9. UV-visible absorption spectrum of *fac*-Ir(ppz)$_3$ in dichloromethane.

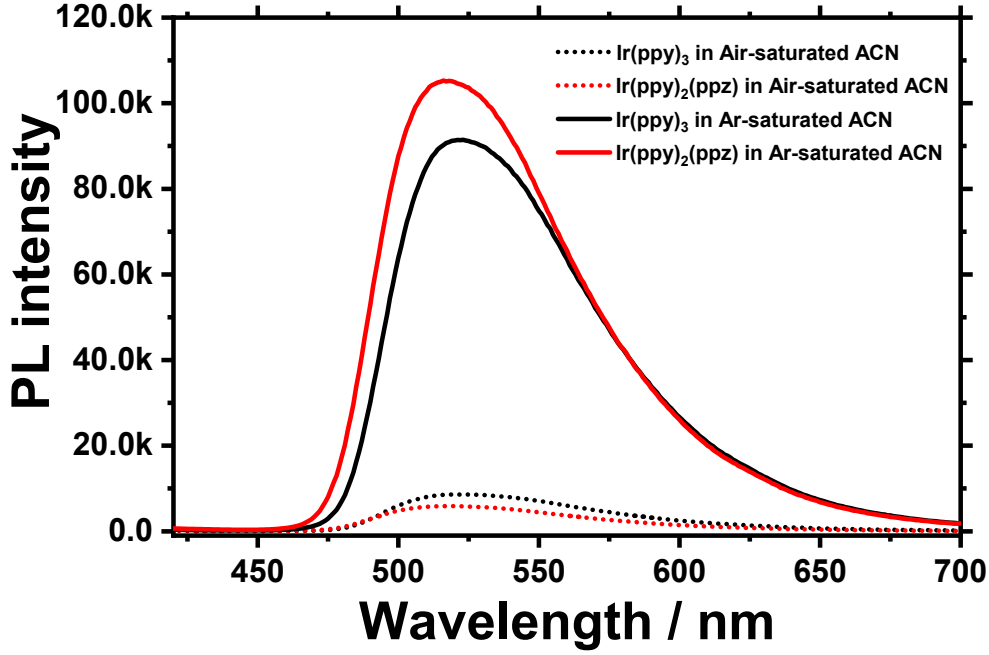

Fig. S10. Emission spectra of *fac*-Ir(ppy)$_3$ and *fac*-Ir(ppy)$_2$(ppz) in Ar-saturated (straight lines) and air-saturated (dotted lines) acetonitrile (ACN). (λ_{Ex} = 400 nm).

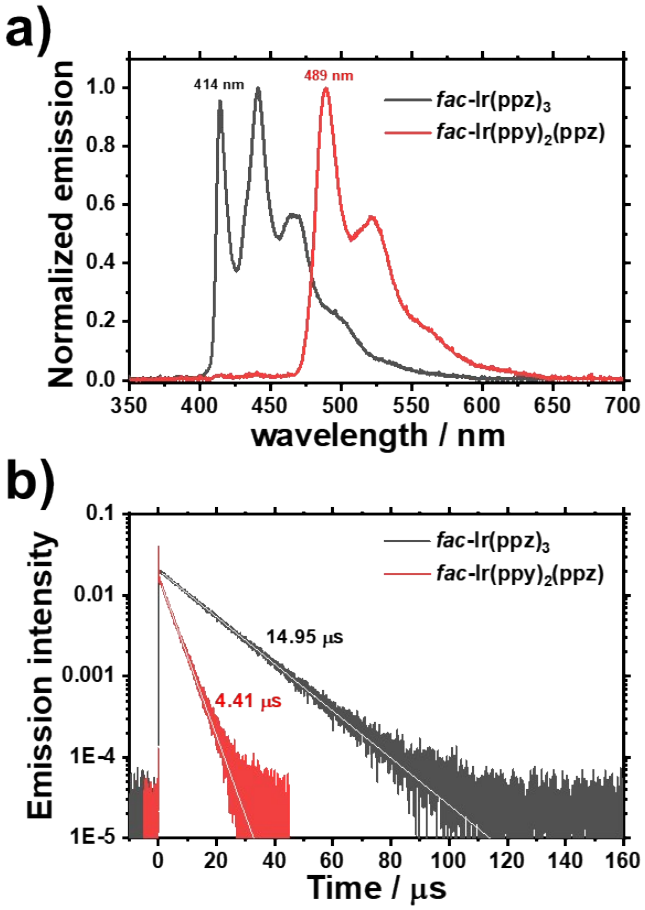

Fig. S11. a) Phosphorescence spectra and b) lifetimes of *fac*-Ir(ppz)$_3$ and *fac*-Ir(ppy)$_2$(ppz) in 2-methyltetrahydrofuran at 77 K.

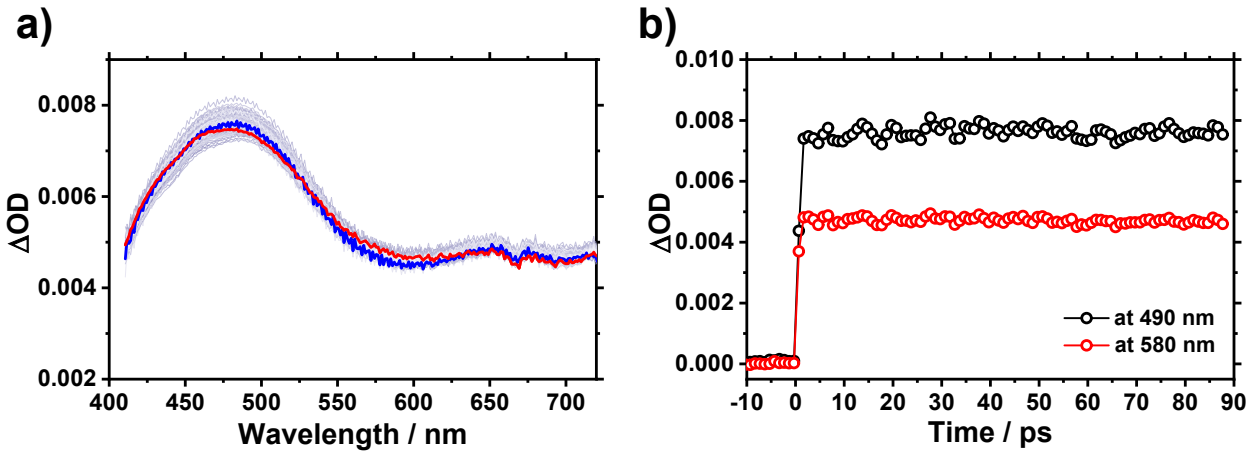

Fig. S12. a) Transient absorption spectra of *fac*-Ir(ppz)$_3$ in acetonitrile (λ_{Ex} = 400 nm). b) Time profile monitored at 490 and 580 nm.

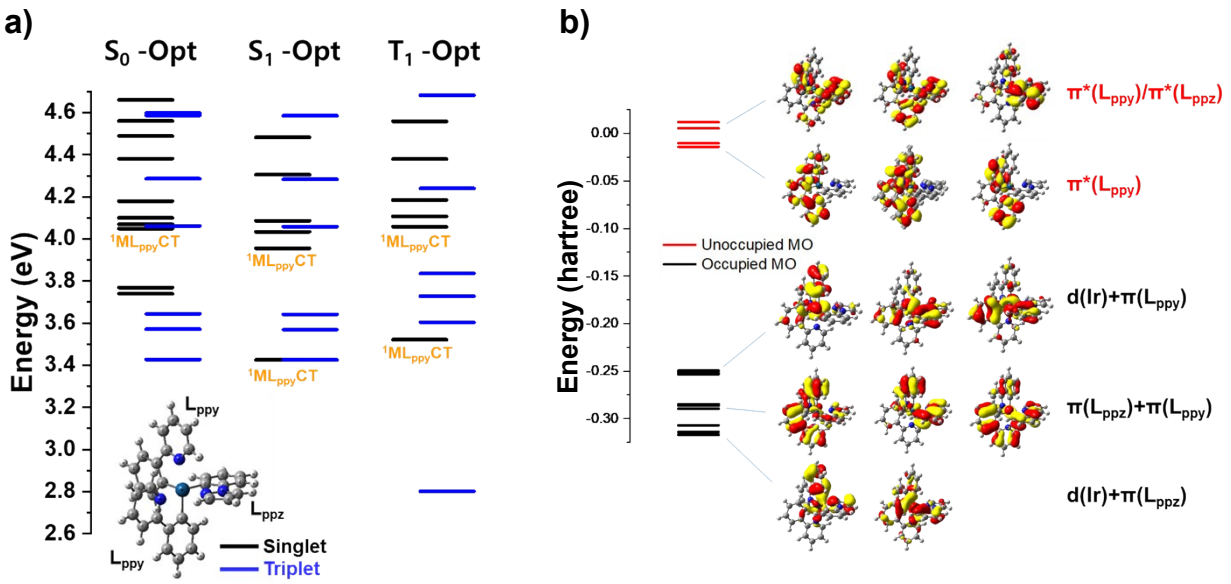

Fig. S13. a) TDDFT-calculated excited state energy levels at the optimized geometries of S_0, S_1, and T_1, states. b) Energy levels of occupied and unoccupied molecular orbitals.

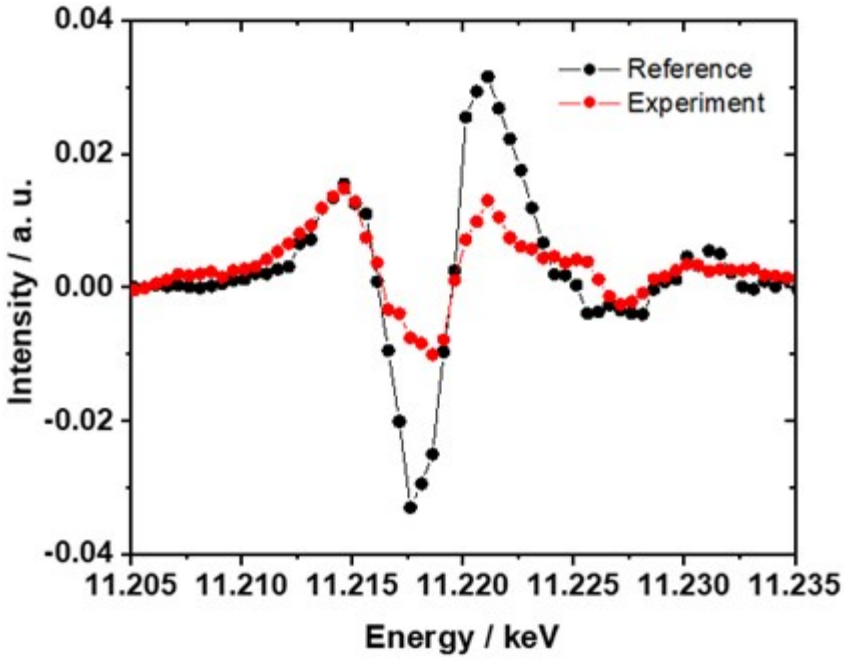

Fig. S14. Difference curves of the reference sample, *fac*-Ir(ppy)$_2$(bpy). The difference curve of *fac*-Ir(ppy)$_2$(bpy) measured in this study is shown as a red circle. The reference curve (black circle) of *fac*-Ir(ppy)$_2$(bpy) was reproduced from ref. 5.

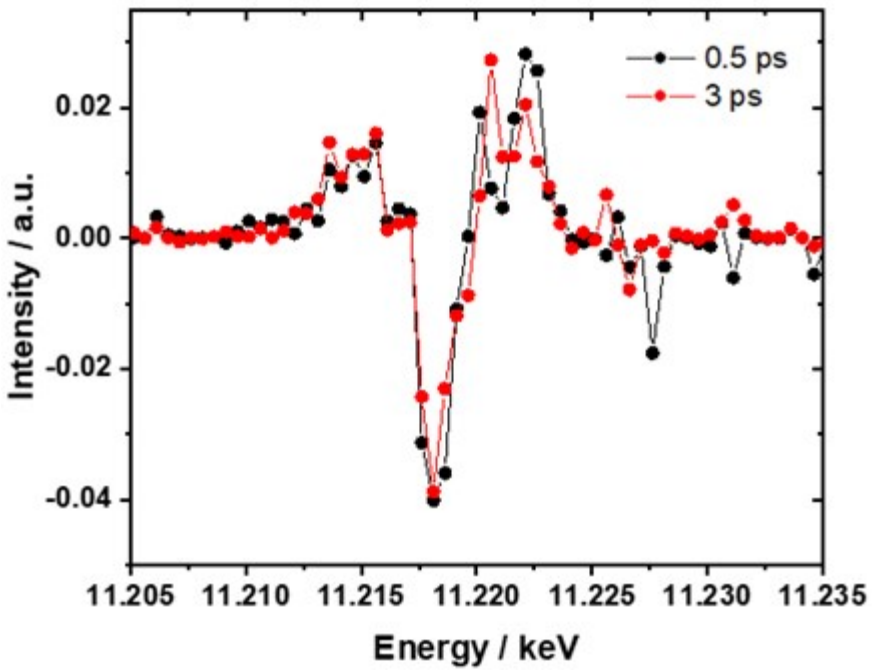

Fig. S15. Reconstructed curves of *fac*-Ir(ppy)$_2$(ppz) measured at Δt = 0.5 and 3.0 ps.

References

1. M. Nonoyama, *B Chem Soc Jpn*, 1974, **47**, 767-768.
2. S. Sprouse, K. A. King, P. J. Spellane and R. J. Watts, *J Am Chem Soc*, 1984, **106**, 6647-6653.
3. A. B. Tamayo, B. D. Alleyne, P. I. Djurovich, S. Lamansky, I. Tsyba, N. N. Ho, R. Bau and M. E. Thompson, *J Am Chem Soc*, 2003, **125**, 7377-7387.
4. K. Dedeian, J. M. Shi, N. Shepherd, E. Forsythe and D. C. Morton, *Inorg Chem*, 2005, **44**, 4445-4447.
5. A. Britz, Ph. D. dissertation, University Hamburg, 2016.
6. M. J. Frisch, G. W. Trucks, H. B. Schlegel, G. E. Scuseria, M. A. Robb, J. R. Cheeseman, G. Scalmani, V. Barone, G. A. Petersson, H. Nakatsuji, X. Li, M. Caricato, A. V. Marenich, J. Bloino, B. G. Janesko, R. Gomperts, B. Mennucci, H. P. Hratchian, J. V. Ortiz, A. F. Izmaylov, J. L. Sonnenberg, D. Williams-Young, F. Ding, F. Lipparini, F. Egidi, J. Goings, B. Peng, A. Petrone, T. Henderson, D. Ranasinghe, V. G. Zakrzewski, J. Gao, N. Rega, G. Zheng, W. Liang, M. Hada, M. Ehara, K. Toyota, R. Fukuda, J. Hasegawa, M. Ishida, T. Nakajima, Y. Honda, O. Kitao, H. Nakai, T. Vreven, K. Throssell, J. A. Montgomery, Jr., J. E. Peralta, F. Ogliaro, M. J. Bearpark, J. J. Heyd, E. N. Brothers, K. N. Kudin, V. N. Staroverov, T. A. Keith, R. Kobayashi, J. Normand, K. Raghavachari, A. P. Rendell, J. C. Burant, S. S. Iyengar, J. Tomasi, M. Cossi, J. M. Millam, M. Klene, C. Adamo, R. Cammi, J. W. Ochterski, R. L. Martin, K. Morokuma, O. Farkas, J. B. Foresman, and D. J. Fox, Gaussian 16 Rev. B.01; Gaussian, Inc., Wallingford, CT, 2016.